Femtosecond parabolic pulse shaping in normally dispersive optical fibers

Igor A. Sukhoivanov,[1,4] Sergii O. Iakushev,[2,6] Oleksiy V. Shulika,[1,2,5] Antonio Díez,[3,7] and Miguel Andrés[3,*]

[1]*Universidad de Guanajuato, Comunidad de Palo Blanco, C.P. 36730, Salamanca, GTO, Mexico*
[2] *Kharkov National University of Radio Electronics, Kharkov 61166, Ukraine*
[3]*Universidad de Valencia, Burjassot (Valencia), Spain*
[4]*i.sukhoivanov@ieee.org*
[5]*a.shulika@ieee.org*
[6]*iakushev@ieee.org*
[7]*antonio.diez@uv.es*
[*]*miguel.andres@uv.es*

Abstract: Formation of parabolic pulses at femtosecond time scale by means of passive nonlinear reshaping in normally dispersive optical fibers is analyzed. Two approaches are examined and compared: the parabolic waveform formation in transient propagation regime and parabolic waveform formation in the steady-state propagation regime. It is found that both approaches could produce parabolic pulses as short as few hundred femtoseconds applying commercially available fibers, specially designed all-normal dispersion photonic crystal fiber and modern femtosecond lasers for pumping. The ranges of parameters providing parabolic pulse formation at the femtosecond time scale are found depending on the initial pulse duration, chirp and energy. Applicability of different fibers for femtosecond pulse shaping is analyzed. Recommendation for shortest parabolic pulse formation is made based on the analysis presented.

©2013 Optical Society of America

OCIS codes: (190.4370) Nonlinear optics, fibers; (320.7110) Ultrafast nonlinear optics; (320.5540) Pulse shaping; (060.5295) Photonic crystal fibers.

References and links

1. S. Boscolo and C. Finot, "Nonlinear pulse shaping in fibres for pulse generation and optical processing," Int. J. Opt. **2012**, 159057 (2012), doi:10.1155/2012/159057.
2. J. M. Dudley, C. Finot, D. J. Richardson, and G. Millot, "Self-similarity in ultrafast nonlinear optics," Nat. Phys. **3**(9), 597–603 (2007), doi:10.1038/nphys705.
3. C. Finot, J. M. Dudley, B. Kibler, D. J. Richardson, and G. Millot, "Optical parabolic pulse generation and applications," IEEE J. Quantum Electron. **45**(11), 1482–1489 (2009), doi:10.1109/JQE.2009.2027446.
4. C. Finot, S. Pitois, and G. Millot, "Regenerative 40 Gbit/s wavelength converter based on similariton generation," Opt. Lett. **30**(14), 1776–1778 (2005), doi:10.1364/OL.30.001776.
5. F. Parmigiani, P. Petropoulos, M. Ibsen, and D. J. Richardson, "Pulse retiming based on XPM using parabolic pulses formed in a fiber Bragg grating," IEEE Photon. Technol. Lett. **18**(7), 829–831 (2006), doi:10.1109/LPT.2006.871848.
6. S. Boscolo, S. K. Turitsyn, and K. J. Blow, "Time domain all-optical signal processing at a RZ optical receiver," Opt. Express **13**(16), 6217–6227 (2005), doi:10.1364/OPEX.13.006217.
7. T. T. Ng, F. Parmigiani, M. Ibsen, Z. Zhang, P. Petropoulos, and D. J. Richardson, "Compensation of linear distortions by using XPM with parabolic pulses as a time lens," IEEE Photon. Technol. Lett. **20**(13), 1097–1099 (2008), doi:10.1109/LPT.2008.924304.
8. P. Petropoulos, M. Ibsen, A. D. Ellis, and D. J. Richardson, "Rectangular pulse generations based on pulse reshaping using a superstructured fiber Bragg grating," J. Lightwave Technol. **19**(5), 746–752 (2001), doi:10.1109/50.923488.
9. D. Krcmarík, R. Slavík, Y. Park, and J. Azaña, "Nonlinear pulse compression of picosecond parabolic-like pulses synthesized with a long period fiber grating filter," Opt. Express **17**(9), 7074–7087 (2009), doi:10.1364/OE.17.007074.

#189766 - $15.00 USD Received 30 Apr 2013; revised 3 Jun 2013; accepted 3 Jun 2013; published 18 Jul 2013
(C) 2013 OSA

10. T. Hirooka, M. Nakazawa, and K. Okamoto, "Bright and dark 40 GHz parabolic pulse generation using a picosecond optical pulse train and an arrayed waveguide grating," Opt. Lett. **33**(10), 1102–1104 (2008), doi:10.1364/OL.33.001102.
11. G. P. Agrawal, Nonlinear Fiber Optics, 3rd ed. (Academic Press, 2001).
12. T. Hirooka and M. Nakazawa, "Parabolic pulse generation by use of a dispersion-decreasing fiber with normal group-velocity dispersion," Opt. Lett. **29**(5), 498–500 (2004), doi:10.1364/OL.29.000498.
13. B. Kibler, C. Billet, P.-A. Lacourt, R. Ferriere, L. Larger, and J. M. Dudley, "Parabolic pulse generation in comb-like profiled dispersion decreasing fibre," Electron. Lett. **42**(17), 965–966 (2006), doi:10.1049/el:20062073.
14. C. Finot, L. Provost, P. Petropoulos, and D. J. Richardson, "Parabolic pulse generation through passive nonlinear pulse reshaping in a normally dispersive two segment fiber device," Opt. Express **15**(3), 852–864 (2007), doi:10.1364/OE.15.000852.
15. S. Boscolo, A. I. Latkin, and S. K. Turitsyn, "Passive nonlinear pulse shaping in normally dispersive fiber systems," IEEE J. Quantum Electron. **44**(12), 1196–1203 (2008), doi:10.1109/JQE.2008.2003494.
16. I. A. Sukhoivanov, S. O. Iakushev, O. V. Shulika, I. V. Guryev, J. A. Andrade Lucio, and O. G. Ibarra Manzano, "Formation of parabolic optical pulses in passive optical fibers," Proc. SPIE **8011**, 801131, 801131-8 (2011), doi:10.1117/12.901822.
17. S. O. Iakushev, O. V. Shulika, and I. A. Sukhoivanov, "Passive nonlinear reshaping towards parabolic pulses in the steady-state regime in optical fibers," Opt. Commun. **285**(21-22), 4493–4499 (2012), doi:10.1016/j.optcom.2012.06.024.
18. K. J. Blow and D. Wood, "Theoretical description of transient stimulated scattering in optical fibers," IEEE J. Quantum Electron. **25**(12), 2665–2673 (1989), doi:10.1109/3.40655.
19. J. Hult, "A fourth-order runge–kutta in the interaction picture method for simulating supercontinuum generation in optical fibers," J. Lightwave Technol. **25**(12), 3770–3775 (2007), doi:10.1109/JLT.2007.909373.
20. C. Finot, F. Parmigiani, P. Petropoulos, and D. J. Richardson, "Parabolic pulse evolution in normally dispersive fiber amplifiers preceding the similariton formation regime," Opt. Express **14**(8), 3161–3170 (2006), doi:10.1364/OE.14.003161.
21. D. Anderson, M. Desaix, M. Lisak, and M. L. Quiroga-Teixeiro, "Wave breaking in nonlinear-optical fibers," J. Opt. Soc. Am. B **9**(8), 1358–1361 (1992), doi:10.1364/JOSAB.9.001358.
22. www.thorlabs.com
23. http://www.nktphotonics.com/lmafibers-specifications
24. S. O. Iakushev, O. V. Shulika, and I. A. Sukhoivanov, "Sub-10-fs Pulses Produced From Compression of Supercontinuum Generated in All-Normal Dispersion Photonic Crystal Fiber," in *Frontiers in Optics Conference/ Laser Science*, Technical Digest (CD) (Optical Society of America, 2012), paper FW3A.41. http://dx.doi.org/10.1364/FIO.2012.FW3A.41
25. M. Koshiba and K. Saitoh, "Applicability of classical optical fiber theories to holey fibers," Opt. Lett. **29**(15), 1739–1741 (2004), doi:10.1364/OL.29.001739.
26. K. Saitoh and M. Koshiba, "Empirical relations for simple design of photonic crystal fibers," Opt. Express **13**(1), 267–274 (2005), doi:10.1364/OPEX.13.000267.
27. B. G. Bale, S. Boscolo, K. Hammani, and C. Finot, "Effects of fourth-order fiber dispersion on ultrashort parabolic optical pulses in the normal dispersion regime," J. Opt. Soc. Am. B **28**(9), 2059–2065 (2011), doi:10.1364/JOSAB.28.002059.
28. A. M. Heidt, J. Rothhardt, A. Hartung, H. Bartelt, E. G. Rohwer, J. Limpert, and A. Tünnermann, "High quality sub-two cycle pulses from compression of supercontinuum generated in all-normal dispersion photonic crystal fiber," Opt. Express **19**(15), 13873–13879 (2011), doi:10.1364/OE.19.013873.
29. A. M. Heidt, A. Hartung, G. W. Bosman, P. Krok, E. G. Rohwer, H. Schwoerer, and H. Bartelt, "Coherent octave spanning near-infrared and visible supercontinuum generation in all-normal dispersion photonic crystal fibers," Opt. Express **19**(4), 3775–3787 (2011), doi:10.1364/OE.19.003775.
30. A. Hartung, A. M. Heidt, and H. Bartelt, "Design of all-normal dispersion microstructured optical fibers for pulse-preserving supercontinuum generation," Opt. Express **19**(8), 7742–7749 (2011), doi:10.1364/OE.19.007742.
31. A. Bartels, D. Heinecke, and S. A. Diddams, "Passively mode-locked 10 GHz femtosecond Ti:sapphire laser," Opt. Lett. **33**(16), 1905–1907 (2008), doi:10.1364/OL.33.001905.
32. H. Byun, M. Y. Sander, A. Motamedi, H. Shen, G. S. Petrich, L. A. Kolodziejski, E. P. Ippen, and F. X. Kärtner, "Compact, stable 1 GHz femtosecond Er-doped fiber lasers," Appl. Opt. **49**(29), 5577–5582 (2010), doi:10.1364/AO.49.005577.
33. G. P. Agrawal, "Effect of intrapulse stimulated Raman scattering on soliton-effect pulse compression in optical fibers," Opt. Lett. **15**(4), 224–226 (1990).
34. Y. Meng, S. Zhang, C. Jin, H. Li, and X. Wang, "Enhanced compression of femtosecond pulse in hollow-core photonic bandgap fibers," Opt. Commun. **283**(11), 2411–2415 (2010).
35. S. Zhou, L. Kuznetsova, A. Chong, and F. Wise, "Compensation of nonlinear phase shifts with third-order dispersion in short-pulse fiber amplifiers," Opt. Express **13**(13), 4869–4877 (2005).

#189766 - $15.00 USD Received 30 Apr 2013; revised 3 Jun 2013; accepted 3 Jun 2013; published 18 Jul 2013
(C) 2013 OSA

1. Introduction

The state of the art ultrafast lasers deliver usually Gaussian or secant pulse waveforms. However, many practical applications require employment of larger variety of pulse waveforms. Flat-top (rectangular-like), triangular, and parabolic pulses are used in all-optical signal processing, ultra-high-speed optical systems, and nonlinear optics [1]. Particularly, the interest on parabolic pulses over recent years was inspired by their unique properties [2]. These pulses propagate self-similarly in an active fiber in the presence of normal dispersion and nonlinearity, and therefore they are termed "similaritons". The amplitude and width scaling in this case depends only on the amplifier parameters and the input pulse energy. Parabolic pulses have found numerous applications in pulse amplification and compression [3] as well as in optical communications [1, 3]. These include among others the optical regeneration [4], the pulse re-timing [5], the optimization of return-to-zero optical receivers [6], and mitigation of the linear waveform distortions [7].

In order to fulfill requirements of telecommunications, the compact fiber-based techniques for pulse shaping are preferable. Several linear- and nonlinear-optical techniques were proposed for this purpose. Linear techniques include application of specially designed super-structured fiber Bragg gratings (FBG) [8], long-period fiber grating filters [9], and arrayed waveguide gratings [10]. For example, FBG is used as a linear filter acting on an input Gaussian or secant optical pulse, and the grating coupling-strength and period profiles are designed to achieve the desired spectral transfer function. Thus, this pulse-shaping strategy is based on the proper manipulation of the spectral-domain features of the input optical pulse in order to obtain the spectral profile that corresponds to the desired temporal profile. The advantage of linear techniques is independence of the pulse reshaping from the input optical pulse power.

Nonlinear techniques utilize complex dynamics of pulse evolution during ultrashort pulse propagation in a fiber with Kerr nonlinearity. The intensity dependence of the refractive index of a fiber leads either to self-phase modulation (SPM) or cross-phase modulation (XPM), depending on the peak power and shape of the input signal. The interplay of group-velocity (second-order) dispersion (GVD) and SPM gives rise to the various scenarios of pulse evolution in the fiber when both pulse shape and spectrum can be drastically changed [11]. Here we consider fibers with normal dispersion; in this case it is possible to obtain a parabolic waveform in the fiber due to the interplay of SPM and GVD. Particularly the application of dispersion decreasing fiber [12, 13] and conventional normally dispersive fiber [14, 15] for obtaining parabolic pulses was reported. In the first case the pulse reshaping is based on the longitudinal decreasing of the normal dispersion in the tapered fibers that is equivalent to presence of linear gain. In the second case the pulse reshaping is based on the interplay of the fixed normal dispersion and SPM; thus conventional single mode fibers can be used for pulse reshaping. The advantage of nonlinear shaping techniques is additional capabilities due to the changing of spectral content, such as spectral broadening or spectral narrowing.

All mentioned approaches however, preliminary deal with picosecond pulses, whereas femtosecond pulses would be more attractive in many telecommunication applications as well as for amplification and compression purposes. To the best of our knowledge the shortest parabolic pulse generated up to know has duration of 540 fs and was obtained applying a comb-like profiled dispersion decreasing fiber [13]. Here we investigate numerically the possibility of femtosecond parabolic pulses generation via nonlinear reshaping in normally dispersive fibers. We examine here two approaches proposed for nonlinear reshaping in the normally dispersive fiber. The first one was proposed by Finot at al [14], and implies parabolic pulse formation as a transient state of pulse evolution in the fiber. The second approach proposed in our group implies parabolic pulse formation in the steady-state regime [16, 17]. We compare here their advantages and disadvantages for femtosecond parabolic pulse shaping, and analyze the applicability of different fibers for femtosecond pulse shaping.

#189766 - $15.00 USD Received 30 Apr 2013; revised 3 Jun 2013; accepted 3 Jun 2013; published 18 Jul 2013
(C) 2013 OSA

2. Theory

It is known that picosecond pulses are well described by nonlinear Schrödinger equation [11]. However, as pulse duration goes down to the femtosecond range, the higher-order nonlinear effects have to be included, namely the pulse self-steepening, and the intrapulse Raman scattering. In this case the pulse propagation equation is frequently referred to as generalized nonlinear Schrödinger equation (GNLSE). It is formulated in terms of the electric field envelope $A = A(z, T)$ in a retarded reference time frame $T = t - \beta_1 z$ like its simplified counterpart, and has the form [11]:

$$\frac{\partial A}{\partial z} = -\frac{\alpha}{2}A - \left(\sum_{n\geq 2}\beta_n \frac{i^{n-1}}{n!}\frac{\partial^n}{\partial T^n}\right)A + i\gamma\left(1+\frac{1}{\omega_0}\frac{\partial}{\partial T}\right) \times\left((1-f_R)A|A|^2 + f_R A\int_0^\infty h_R(\tau)|A(z,T-\tau)|^2\, d\tau\right), \tag{1}$$

where α is the attenuation constant, γ is the nonlinear coefficient, β_n are the dispersion coefficients obtained by a Taylor series expansion of the propagation constant $\beta(\omega)$ around the pulse center frequency ω_0. The pulse center frequency corresponds to the wavelength of 800 nm in our study. The response function $R(t) = (1-f_R)\delta(t) + f_R h_R(t)$ includes both the instantaneous electronic and delayed Raman contributions, with $f_R = 0.18$ representing the fractional contribution of the delayed Raman response. For the Raman response function of the silica fiber, $h_R(t)$, the analytical expression is used [18]:

$$h_R(t) = \frac{\tau_1^2+\tau_2^2}{\tau_1\tau_2}\exp\left(-\frac{t}{\tau_2}\right)\sin\left(\frac{t}{\tau_1}\right), \tag{2}$$

where $\tau_1 = 12.2$ fs and $\tau_2 = 32$ fs.

The GNLSE (1) is solved by Runge–Kutta in the interaction picture method [19].

In general case the pulse launched into the fiber can include the time dependence of the instantaneous frequency, i.e. be chirped. We include chirp in the initial pulse in the following way:

$$A_{chirp} = A_{unchirp}\exp\left(iC\frac{T^2}{2T_0^2}\right), \tag{3}$$

where $A_{unchirp}$ is the waveform of an unchirped initial pulse; C is the chirp parameter; T_0 is the initial pulse duration (half-width at 1/*e*-intensity level) which is nominally 100 fs in the paper. This leads to the linear dependence of instantaneous frequency $\omega = \omega_0 + CT/T_0^2$ (linear chirp).

Pulse reshaping towards parabolic waveform during its propagation in the fiber is analyzed using a misfit parameter *M*, which shows the deviation between the pulse temporal intensity profile $|A(T)|^2$ and a parabolic fit $|A_p(T)|^2$ of the same energy [20]:

$$M = \frac{\int\left(|A|^2 - |A_p|^2\right)^2 d\tau}{\int |A|^4\, d\tau}. \tag{4}$$

#189766 - $15.00 USD Received 30 Apr 2013; revised 3 Jun 2013; accepted 3 Jun 2013; published 18 Jul 2013
(C) 2013 OSA

The expression for the parabolic pulse with an energy $E_p = 4P_pT_p/2\sqrt{3}$ is given by:

$$\begin{cases} A_p(T) = \sqrt{P_p}\sqrt{1-2T^2/T_p^{\,2}}, & |T| \le T_p/\sqrt{2} \\ A_p(T) = 0, & |T| > T_p/\sqrt{2} \end{cases}, \quad (5)$$

where P_p is the peak power of the parabolic pulse, T_p is the duration of the parabolic pulse. The misfit parameter M allows estimating pulse shape imperfection as compared to the parabolic shape; the less value of M shows better fit to the parabolic waveform. We consider the pulse shape is parabolic enough when $M < 0.04$.

We consider here two approaches for obtaining parabolic pulses via nonlinear reshaping in the normal dispersive fiber. The first one, hereafter Approach **A**, implies that parabolic pulses can be obtained at the short propagation distance in the fiber preceding the optical wave breaking length (ξ_{OWB}) [14]. In this case pulse reshaping appears very fast due to the strong action of the self-phase modulation (SPM), which at first can lead to the appearing of the parabolic waveform but then pulse shape can become rectangular and even optical wave breaking can appears [21]. The analysis of pulse reshaping in this case usually is made for fiber length less than the dispersion length ($L_D = T_0^2/|\beta_2|$) $z \le L_D$. The parabolic waveforms generated this way, represent transient states of the nonlinear pulse evolution in the fiber. Thus, they have a finite life time; therefore stabilization of the parabolic features is required [14].

The second approach, hereafter Approach **B**, implies that pulse reshaping towards parabolic waveform appears in the steady-state regime, i.e. at the longer propagation distances ($z > L_D$) which, qualitatively speaking, are exceeding substantially the optical wave breaking length ξ_{OWB} [16]. Qualitative definition of the steady-state regime the criterion based on the derivative of the misfit parameter *M* over the normalized propagation distance ξ. The condition $|\partial M(\xi)/\partial\xi| \le 5\cdot10^{-3}$ identifies the border when changes of the pulse shape become small enough to be negligible. When this criterion is satisfied the pulse spectral width is already very close to the asymptotic value, e.g. in the case of initial secant pulse $\partial M(\xi)/\partial\xi = 5\cdot10^{-3}$ corresponds already to the 97% from the asymptotic spectral width [17]. The pulse reshaping in this case occurs under the domination of the normal dispersion which leads to the considerable reduction of the pulse peak power due to dispersion broadening, and thus, results in much weaker action of SPM. In this case both the pulse temporal profile and the spectral profile are changing very slowly and pulse chirp becomes linear. Under the special initial conditions, which are easily achievable, the pulse shape can become parabolic in this regime, and what is more important, remains parabolic during further pulse propagation in the fiber. Thus, this regime is very similar to the asymptotic propagation of similaritons in fiber amplifiers (excepting for the pulse amplification) [2].

3. Fibers and pulses

Parabolic pulse formation needs two ingredients: fiber nonlinearity and normal dispersion at the central frequency of the incident pulse [14–17]. We can always find wavelength range where any fiber demonstrates normal dispersion. This is due to very large contribution of the material dispersion to the total dispersion of the fiber in the short wavelength side. If we are talking about microstructured optical fibers, they can demonstrate normal dispersion not only at the short wavelengths, but at the middle and long wavelengths as well, thanks to specially designed waveguide dispersion. However, the choice of the wavelength range is always restricted by the wavelength of the ultrafast oscillator available, thus making this freedom

#189766 - $15.00 USD Received 30 Apr 2013; revised 3 Jun 2013; accepted 3 Jun 2013; published 18 Jul 2013
(C) 2013 OSA

illusory one. In this study we are interested in wavelength range around 800 nm and suitability of various single-mode fibers, both commercial and custom made, for the parabolic pulse formation under 800 nm pump. This interest together with conditions outlined above predetermines our choice of the fibers. For analysis of parabolic pulse formation we have chosen three different fibers Thorlabs 780HP [22], LMA15 [23], and specially designed all-normal dispersion photonic crystal fiber (ANDi PCF) which demonstrate normal dispersion at 800 nm [24]. Two of those fibers, 780HP and LMA15, are representatives of the fiber market. The third one represents a kind of fibers which attracted attention recently in context of special kind supercontinuum generation [24]. Figure 1(a) shows spectral dependence of the dispersion parameter *D* for all three fibers. The dispersion profiles of the fibers 780HP and LMA15 are adopted from the experimental curves provided by manufacturers, while dispersion curve of the ANDi PCF is calculated with the analytical method described in [25, 26]. Three kinds of fibers, chosen for our study, represent typical dispersion profiles of the silica fibers with realistic designs, not futuristic one. The only example missed here is so called ultraflattened-dispersion fiber and its variation the S-profile fiber. However, this kind of fibers is usually oriented on the wavelength range around 1550 nm. Therefore, they are demonstrating special dispersion profile only within few-hundreds nanometer range around 1550 nm, possessing normal dispersion at 800 nm and dispersion profile like that one of conventional single-mode fibers. Thus, suitability of these fibers for fs-parabolic pulse shaping can be estimated starting from results presented for three fibers mentioned above.

Fibers' parameters used in simulations are shown in Table 1. Dispersion coefficients β_n are calculated from $D(\lambda),[\mathrm{ps}/(\mathrm{nm}\cdot\mathrm{km})]$, whereas nonlinear coefficient γ is calculated from the mode field diameter of the fiber using nonlinear refractive index of the silica $n_2 = 3\times10^{-20}\,\mathrm{m}^2/\mathrm{W}$. The designed ANDi PCF has the fused silica solid core and hexagonal lattice of air holes in the cladding region, with pitch $\Lambda = 1\mu\mathrm{m}$ and a relative hole size $d/\Lambda = 0.5$. However, these parameters can vary due to various experimental factors during the drawing process. Figure 1(b) shows the cross-section and the core of the designed ANDi-PCF sample which demonstrate Λ = 1.0 μm and d = 0.53 μm. Although hole's diameter is a little bit larger than nominal value, we do not expect big variations of the dispersion curve. Therefore, calculated data are used.

We have taken into account dispersion coefficients up to 4-th order, because both 3-rd and 4-th order dispersion can influence on the pulse reshaping [17, 27]. On the other hand, four terms of the Taylor expansion are enough to fit the spectral dependence of propagation constant in the fiber considered here. During simulations we neglect the fiber's loss because only short pieces of the fiber are considered here.

In this study we are using two shapes of the incident pulse, the Gaussian and the hyperbolic secant waveform with central wavelength 800 nm. These pulses are similar to that one produced by typical Ti:Sapphire lasers or Erbium-doped fiber lasers with second harmonic generation. Duration of the launched pulses used in our simulations is conditioned by characteristics of the Ti:Sapphire laser system which we will use for experimental realization of the studies presented here. The shortest pulse measured is about 60 fs. And depending on the tuning of intracavity dispersion pulses of 70 – 100 fs duration can be easily produced. The optical scheme for laser-to-fiber coupling does not imply optical components between the laser output and the fiber except the focusing objective. Therefore, only linear chirp can be expected in the pulses incident to the fiber. The amount of initial chirp for a given initial pulse width in our simulations is chosen always such that pulse spectral width corresponds to that one for the transform-limited pulse of 50 fs pulse duration. Thus, we imply that 50 fs pulse is a transform limited one with minimal pulse duration delivered from the laser, whereas imperfect dispersion compensation inside the resonator or impact of outside dispersion produces broadened chirped pulses. We used here pulses with positive

#189766 - $15.00 USD Received 30 Apr 2013; revised 3 Jun 2013; accepted 3 Jun 2013; published 18 Jul 2013
(C) 2013 OSA

chirp, because usually one can expect the presence of positive chirp in the pulse due to the impact of normal material dispersion in optical elements. However, in case of negative chirp one can also obtain quite similar parabolic pulses, as we demonstrated previously [17] for stationary case and in [15] for transient propagation regime.

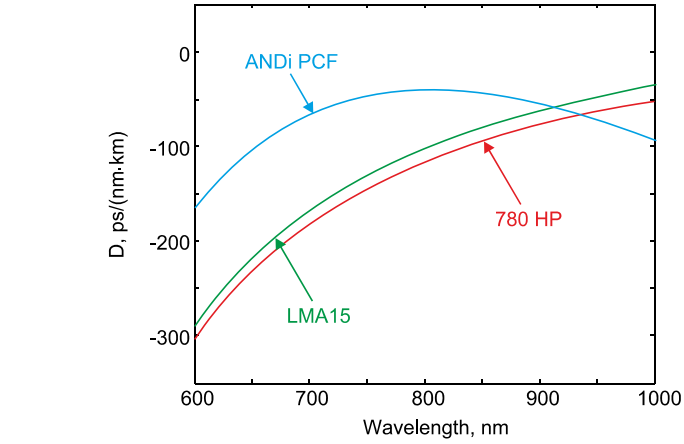

(a)

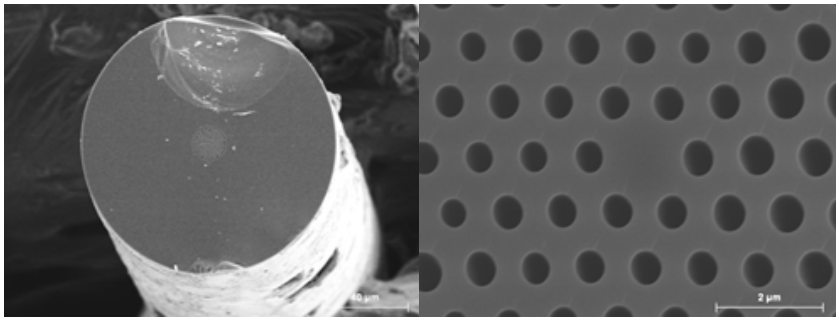

(b)

Fig. 1. (a) Spectral dependence of dispersion parameter D for fibers used in simulations (Thorlabs 780HP, LMA15, and ANDi PCF). (b) Microphotography of the cross-section and the core of the designed ANDi-PCF, Λ = 1.0 μm and d = 0.53 μm

Table 1. Fibers' parameters at the wavelength 800 nm used in simulations

	Thorlabs 780HP	**LMA15**	**ANDi PCF**
β_2, ps^2 / km	3.973×10^{1}	3.49×10^{1}	1.363×10^{1}
β_3, ps^3 / km	2.62×10^{-2}	2.9×10^{-2}	-8.65×10^{-3}
β_4, ps^4 / km	-6.7×10^{-6}	-1.35×10^{-5}	1.674×10^{-4}
γ, 1/(W · km)	12	1.9	113.3

4. Parabolic pulse formation in the conventional single-mode fiber

As a representative of the conventional single-mode fibers available commercially we have chosen Thorlabs 780HP fiber intended for application at near infrared wavelengths. Fiber's parameters used in simulations are shown in Table 1. Pulse duration was varied in the range 70-150 fs (with chirp or without chirp), pulse energy - in the range from a few hundred pJ till a few nJ. Because the state of the art ultrafast lasers deliver usually Gaussian or secant pulses we consider here both Gaussian and secant waveforms for the initial pulse.

#189766 - $15.00 USD Received 30 Apr 2013; revised 3 Jun 2013; accepted 3 Jun 2013; published 18 Jul 2013
(C) 2013 OSA

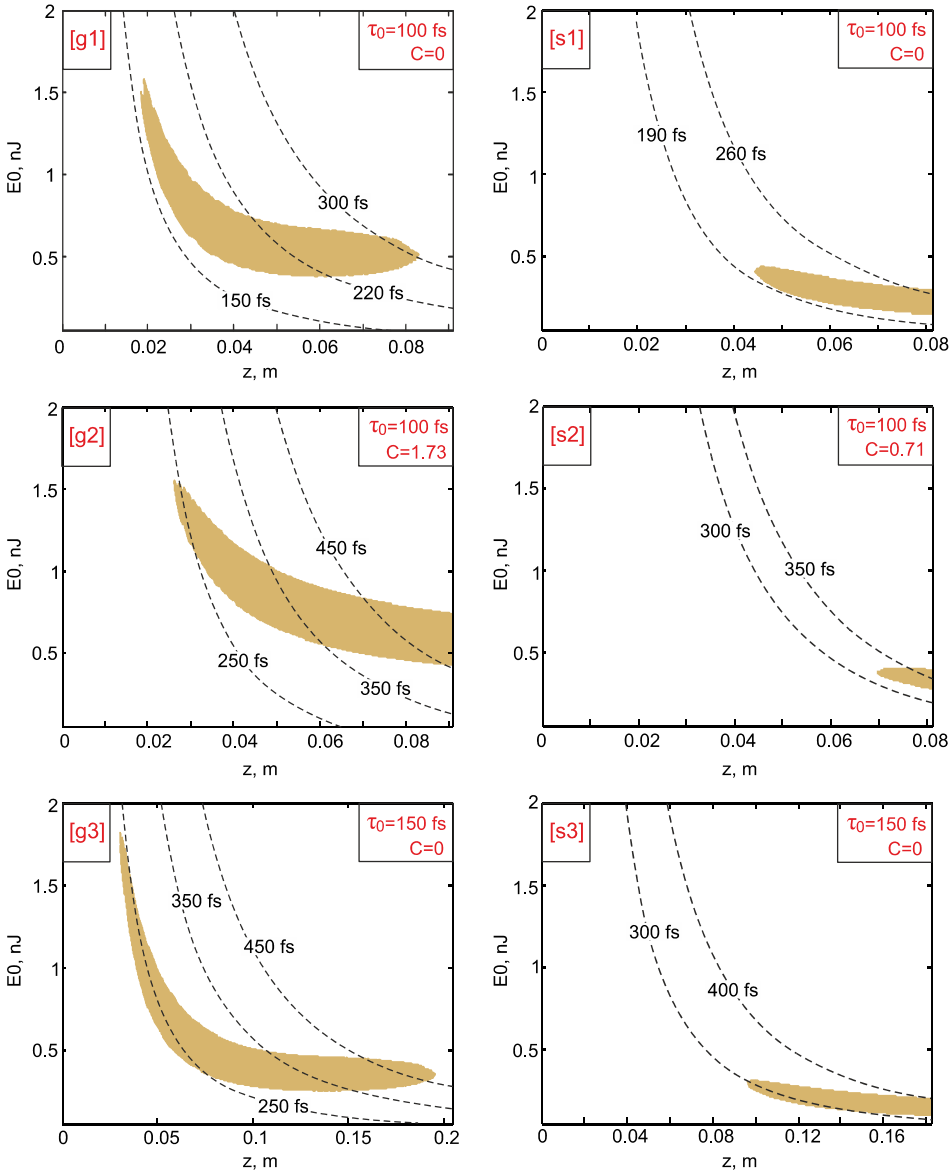

Fig. 2. Misfit parameter maps $M(E_0,\tau)$ and contour curves of pulse duration $\tau(E_0,z)$ (dashed lines) for the case $z \le L_D$. The left column ([g1], [g2], [g3]) shows results for initial Gaussian pulse varying initial pulse duration τ_0 (FWHM) and initial pulse chirp C; right column ([s1], [s2], [s3]) shows results for initial secant pulse. The insets located in the upper right corner show the amount of initial pulse width (FWHM) and chirp.

We analyze femtosecond parabolic pulse formation using calculated maps of the misfit parameter $M(E_0,z)$ and contour curves of pulse duration $\tau(E_0,z)$ in terms of its FWHM, where E_0 is the initial pulse energy and z is the propagation distance in the fiber. Superposition of those characteristics onto the one image allows finding the ranges of parameters where parabolic pulses are formed and, simultaneously, analyzing the duration of parabolic pulses. Figure 2 shows $M(E_0,z)$ and $\tau(E_0,z)$ calculated at the short propagation

#189766 - $15.00 USD Received 30 Apr 2013; revised 3 Jun 2013; accepted 3 Jun 2013; published 18 Jul 2013
(C) 2013 OSA

distance $z \le L_D$ (Approach **A**). The results presented are obtained for two different initial pulse waveforms (Gaussian or secant), different initial pulse duration and initial chirp. The filled areas show the range of parameters where pulse shape becomes parabolic ($M \le 0.04$). The amount of initial chirp for a given initial pulse width is chosen as described above.

From Fig. 2(g1) we can see that from initial unchirped 100 fs Gaussian pulse one can obtain quite short parabolic pulses (160-300 fs) for initial pulse energy 0.4-1.5 nJ. Fiber length has to be quite small 2.5-8 cm fiber. From practical point of view utilizing of such short fibers can be quite difficult. However, recently experimental results with much shorter fiber piece were reported [28], where authors used 1.7 mm of the fiber for supercontinuum generation and compression. Thus, fiber lengths of 2.5-8 cm can be used indeed in the practice. For the same secant pulse (Fig. 2(s1)) the filled area becomes smaller and they are shifted towards longer fiber lengths and lower energies, because the secant shape varies stronger from the parabolic one, and thus, pulse needs longer distance to be transformed. However, in this case it is also possible to obtain ~200 fs parabolic pulses. Introducing a chirp to the initial pulse leads also to the shifting of the filled areas towards longer fiber lengths for both the Gaussian and the secant pulses [Figs. 2(g2), 2(s2)]. Thus the final parabolic pulse duration increases as compared to the initial unchirped pulses. Reshaping of longer initial pulses is shown in Figs. 2(g3), 2(s3). In this case dispersion length becomes larger and we can see that filled areas are shifted towards longer fiber lengths and they are also stronger stretched over the fiber length. This finally also leads to the increasing of the parabolic pulse duration.

Thus, we can conclude that in the case of Approach **A**, it is preferable to use unchirped pulses with shorter initial pulse duration in combination with short fiber pieces (a few cm).

Figure 3 shows the dependence of the misfit parameter M on the initial pulse energy and fiber length z obtained in the steady-state regime when $z > L_D$. This case we are referring to as Approach **B**. We restrict here the maximal fiber length by $L_D < z < 4L_D$, because longer propagation distance leads to a stronger pulse broadening. Only chirped initial pulses are considered here, because evolution of unchirped Gaussian and secant pulses does not tend to the parabolic waveform in the steady-state regime [17].

From Fig. 3(g1) we can see that from initial 100 fs Gaussian pulse one can obtain parabolic pulses with duration as short as 600 fs for initial pulse energy 0.3-0.6 nJ; fiber length has to be at least 12 cm. From secant initial pulse, Fig. 3(s1), one can obtain shorter parabolic pulse (~500 fs) in the steady-state regime at the similar fiber length, but smaller initial pulse energy has to be used. Reducing the initial pulse width (and the corresponding chirp) allows obtaining shorter parabolic pulses in the steady-state regime [Figs. 3(g2), 3(s2)]. However, in the case of secant pulse the filled area is narrowed with increasing of propagation distance; thus the steady-state regime is less stable here. This is due to the insufficient initial chirp, as for secant waveform one has to use stronger initial chirp [17].

Thus, we can conclude that in the steady-state regime we can also obtain femtosecond parabolic pulses (>500 fs) applying initially chirped pulses and fiber length more than 10 cm. A common feature is that for obtaining shorter pulses one has to use shorter initial pulses. However, shorter fibers have to be used in this case especially for Approach **A** (a few cm and less). Another important result is that parabolic pulses both at the short propagation distance and in the steady-state regime are obtained within quite narrow ranges of pulse energy.

#189766 - $15.00 USD Received 30 Apr 2013; revised 3 Jun 2013; accepted 3 Jun 2013; published 18 Jul 2013
(C) 2013 OSA

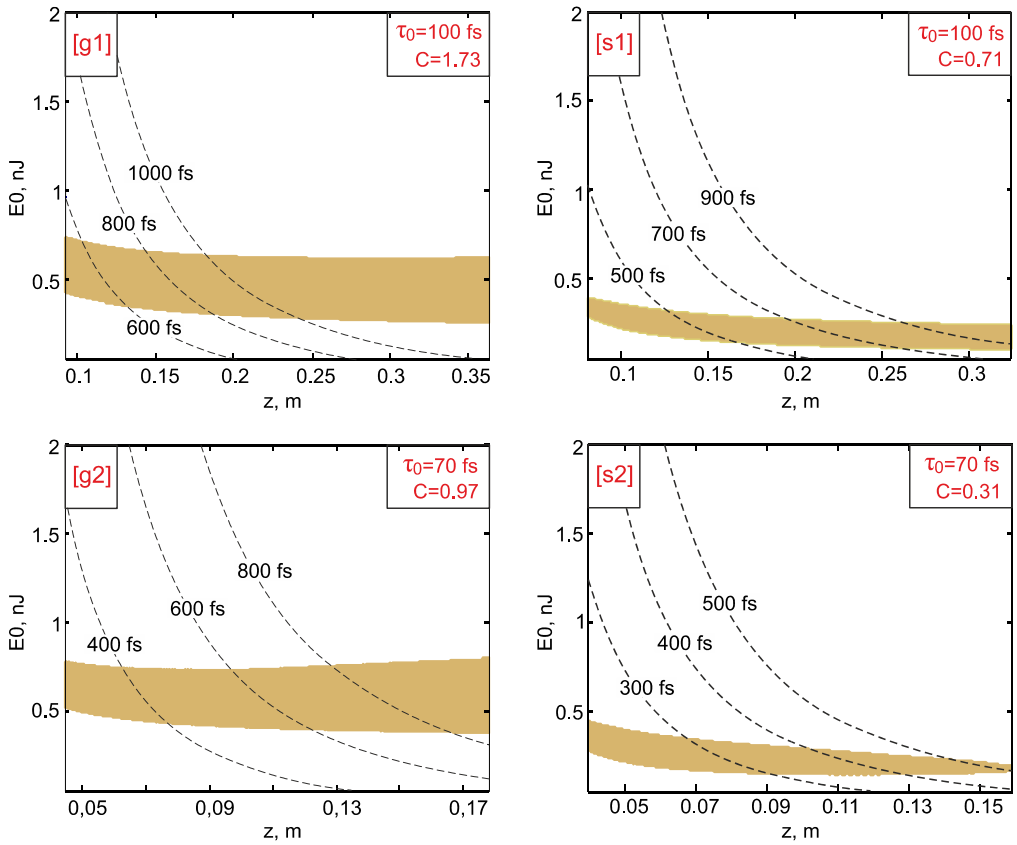

Fig. 3. Misfit parameter maps $M(E_0, \tau)$ and contour curves of pulse duration $\tau(E_0, z)$ (dashed lines) for the case $L_D < z < 4L_D$. The left column ([g1], [g2]) shows results for initial Gaussian pulse varying initial pulse duration τ_0 (FWHM) and initial pulse chirp C, right column ([s1], [s2]) shows results for initial secant pulse. The insets located in the upper right corner show the amount of initial pulse width (FWHM) and chirp.

One can see that in Thorlabs 780HP one can achieve parabolic pulses in the range of initial pulse energy located within 0.1-1.5 nJ. For the tailoring of this operation range and pulse reshaping of smaller or larger pulse energy one can use other fibers.

5. Parabolic pulse formation in the large mode area fiber

Pulses with larger initial pulse energy can be produced applying fiber with smaller nonlinear coefficient. Here we examined a large mode area fiber LMA15. Fiber's parameters used in simulations are shown in Table 1. Figure 4 shows the dependence of the misfit parameter M on the initial pulse energy and fiber length z in this case.

During the simulation we have observed that behavior of the misfit maps against variation of the pulse duration is mainly similar to that one for Thorlabs 780HP. The similarity of results we attribute to the similarity of dispersion characteristics of those fibers. Taking this into consideration we have presented results only for single duration of the initial pulse, which shall be enough to discuss difference to the case of conventional single-mode fiber presented above (Thorlabs 780HP). Also results for the short propagation distance and in the steady-state regime are combined in the same figure.

#189766 - $15.00 USD Received 30 Apr 2013; revised 3 Jun 2013; accepted 3 Jun 2013; published 18 Jul 2013
(C) 2013 OSA

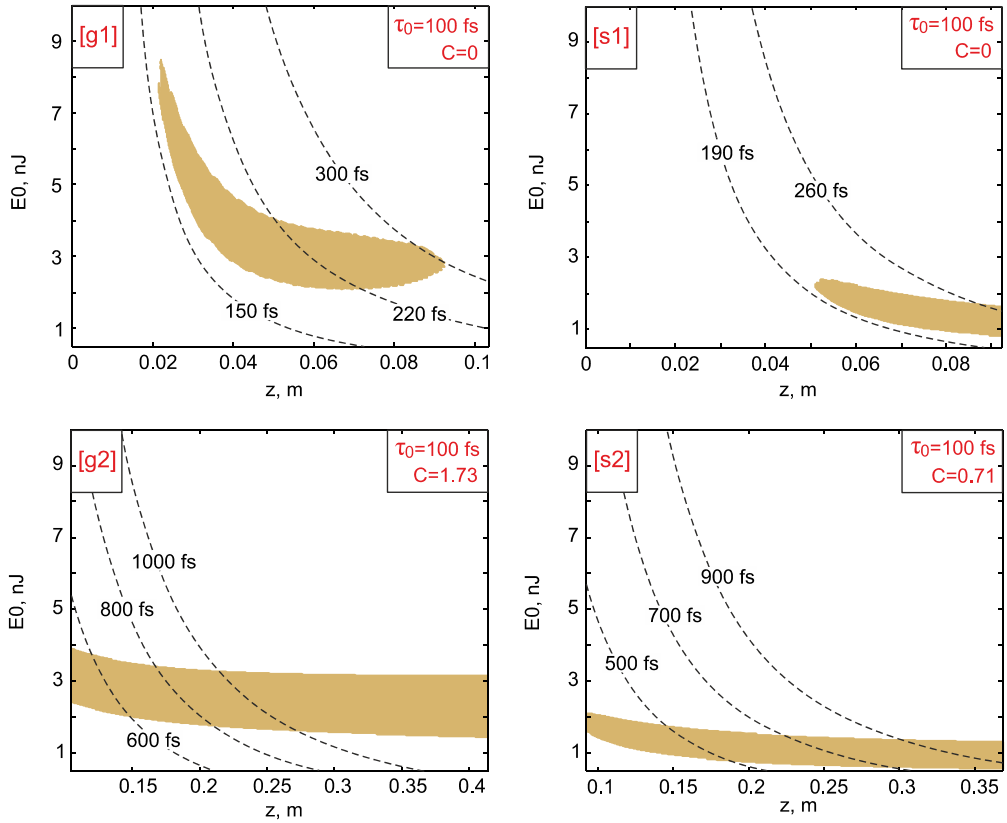

Fig. 4. Misfit parameter maps $M(E_0, \tau)$ and contour curves of pulse duration $\tau(E_0, z)$ (dashed lines). Top row ([g1], [s1]) shows results for the case $z \le L_D$, bottom row ([g2], [s2]) - for $L_D < z < 4L_D$. The left column ([g1], [g2]) shows results for initial Gaussian pulse, right column ([s1], [s2]) - for initial secant pulse. The insets located in the upper right corner show the amount of initial pulse width (FWHM) and chirp.

From Fig. 4 we can see that application of the large mode area fiber indeed allows producing of parabolic pulses with larger pulse energy, whereas similar fiber pieces have to be used and durations of produced parabolic pulses are nearly the same as for Thorlabs 780HP. Thus, application of LMA15 allows tuning the operation range towards larger pulses energies up to 0.8-8 nJ. Application of large mode area fiber with smaller nonlinear coefficient (LMA20, LMA25, LMA35) allows further scaling of pump pulse energy.

6. Parabolic pulse formation in highly nonlinear all-normal dispersion fiber

Finally we investigate parabolic pulse formation in highly nonlinear microstructured fibers. Recently it was demonstrated that novel all-normal dispersion photonic crystal fiber (ANDi PCF) is very attractive for supercontinuum generation [28, 29]. Owing to its unique properties such fiber can be also interesting for nonlinear pulse reshaping. ANDi PCFs possess some very attractive features: 1) Even very short pulses with large spectral bandwidth can be reshaped because of normal dispersion spans over the whole spectral range; 2) ANDi PCF demonstrates a flat-top dispersion profile, pumping in this region reduces impact of higher order dispersion on the reshaping process which is also important for very short pulses; 3)

#189766 - $15.00 USD Received 30 Apr 2013; revised 3 Jun 2013; accepted 3 Jun 2013; published 18 Jul 2013
(C) 2013 OSA

dispersion profile can be tuned such that to provide desired flat-top region in the wide spectral band from visible till near infrared [30].

Recently we have shown that this fiber is well suited for supercontinuum generation at 800 [24]. Here we have investigated pulse reshaping applying this fiber. Fiber's parameters used in simulations are shown in Table 1. Figure 5 shows the dependence of the misfit parameter M on the initial pulse energy and fiber length z for the ANDi PCF. Results for the short propagation distance and in the steady-state regime are combined in the same figure.

From Fig. 5 we can see that parabolic pulses are formed here at the smaller energy namely in the pJ range (9-80 pJ). This is due to the larger nonlinear coefficient in ANDi PCF as compared to the previously considered fibers. Owing to that the designed ANDi PCF can be used for nonlinear reshaping with GHz femtosecond lasers which usually generate pJ pulses [31, 32]. Another important feature is that this fiber provides smaller amount of normal dispersion (β_2). Owing to that dispersion length here is larger for given pulse duration. Practically this allows using of shorter initial pulses while keeping fiber length sufficiently large for easy-to-use operation. For example, here (Fig. 5) we used initial 80 fs pulses and one can see that for the same fiber length than in previous cases, in this case we can obtain shorter pulses as compared to the Thorlabs 780HP or LMA15. Another interesting feature is the expanding of the filled area towards larger energies for chirped Gaussian pulse in the steady-state regime [Fig. 5(g2)]. However, this expansion appears at longer propagation distance and duration of parabolic pulses exceeds 900 fs.

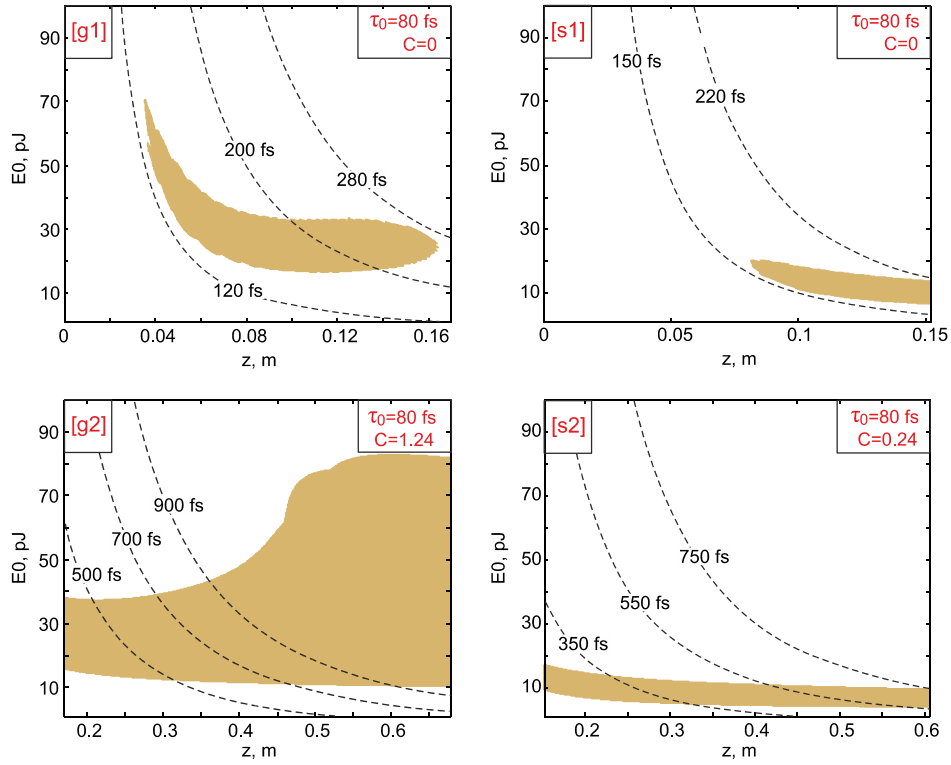

Fig. 5. Misfit parameter maps $M(E_0, \tau)$ and contour curves of pulse duration $\tau(E_0, z)$ (dashed lines). Top row ([g1], [s1]) shows results for the case $z \le L_D$, bottom row ([g2], [s2]) - for $L_D < z < 4L_D$. The left column ([g1], [g2]) shows results for initial Gaussian pulse, right column ([s1], [s2]) - for initial secant pulse. The insets located in the upper right corner show the amount of initial pulse width (FWHM) and chirp.

#189766 - $15.00 USD Received 30 Apr 2013; revised 3 Jun 2013; accepted 3 Jun 2013; published 18 Jul 2013
(C) 2013 OSA

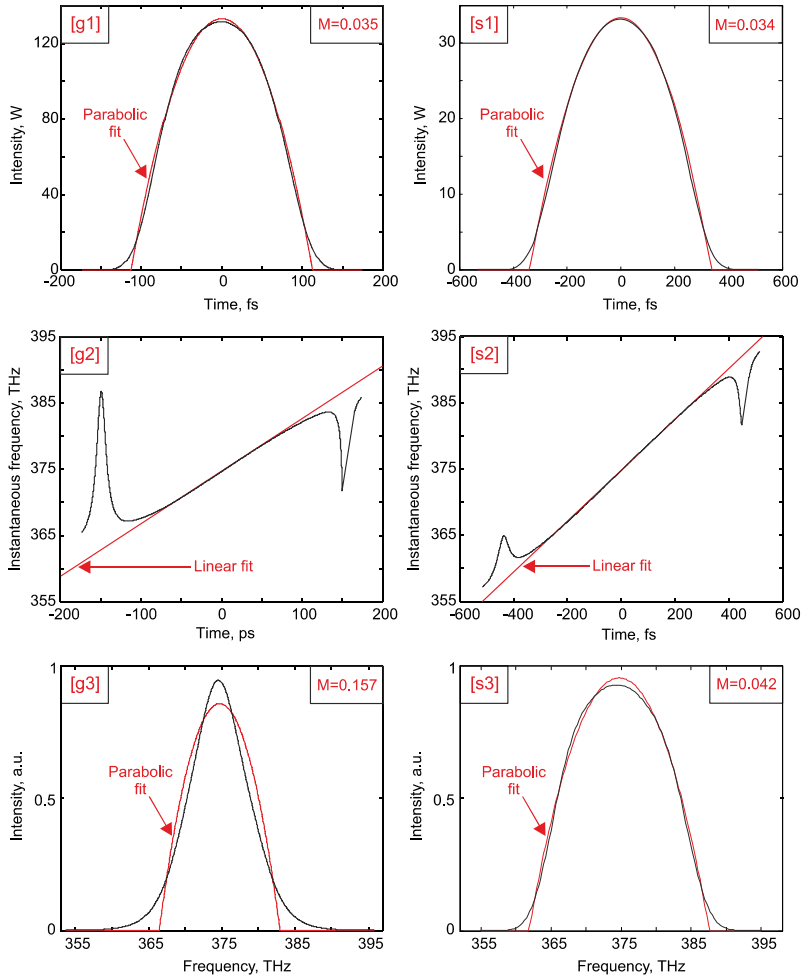

Fig. 6. Parabolic pulses generated in the ANDi PCF. The left column ([g1], [g2], [g3]) shows results (temporal intensity, chirp, spectrum) for parabolic pulse generated at the fiber length 10 cm from initial unchirped Gaussian pulse ($\tau_0 = 80$ fs, $E_0 = 20$ pJ). Right column ([s1], [s2], [s3]) parabolic pulse generated in the steady-state regime at the fiber length 30 cm from initial chirped Gaussian pulse ($\tau_0 = 80$ fs, $E_0 = 15$ pJ, $C = 1.24$). The insets located in the upper right corner show the amount of misfit parameter *M*.

From misfit parameter maps $M(E_0, z)$ and contour curves of pulse duration $\tau(E_0, z)$ presented e.g. in Fig. 5 one can find the shortest parabolic pulses available for the given fiber and initial pulse parameters. A common feature of the contour curves is that $\tau(E_0, z)$ increases nonlinearly with increasing the pulse energy. This occurs due to the stronger impact of nonlinearity on the pulse broadening for larger initial pulse energies. Practically it means that for a given map of the misfit parameter $M(E_0, z)$, it is more preferable to operate at the lower pulse energy (the bottom of the filled area), because parabolic pulses duration is shorter here for a given fiber length.

Keeping in mind the last observation, we have calculated two examples of parabolic pulses found from misfit parameter maps presented in Figs. 5(g1), 5(g2). Figure 6 shows characteristics of these parabolic pulses obtained from 80 fs Gaussian pulse both at the short propagation distance and in the steady-state regime. From Fig. 6 we can see that both

#189766 - $15.00 USD Received 30 Apr 2013; revised 3 Jun 2013; accepted 3 Jun 2013; published 18 Jul 2013
(C) 2013 OSA

parabolic pulses [Figs. 6(g1), 6(s1)] indeed are very close to the ideal parabolic fit profile. However, at the short propagation distance (10 cm) pulse width (FWHM) is 156 fs; in the steady-state regime (30 cm) it is larger, 466 fs, due to the longer propagation distance in the fiber required for appearance of the steady-state regime. However, longer propagation distance in the fiber provides more linear chirp over the whole pulse width [see Figs. 6(g2, s2)], which is more preferable for efficient pulse compression. In the steady-state regime the spectrum obtained is also very close to the ideal parabolic profile [Fig. 6(s3)], whereas at the short propagation distance the spectral profile strongly differs from the parabolic one [Fig. 6(g3)]. From Fig. 5(g2) one can see that shorter propagation distance can be taken in the steady-state regime (e.g. 20 cm), in order to obtain shorter parabolic pulses, but in this case stronger deviation of the spectral profile from a parabolic one is observed.

Thus, we can conclude that main advantage of Approach **A** is formation of very short parabolic pulses with broadening factor ~2. Minimal width of parabolic pulses in this case is limited generally by the width of the initial pulses. However, very short fiber is also required (a few cm) to obtain shortest parabolic pulses. In this case it is reasonable to use fibers with smaller amount of second order dispersion which allows using of shorter initial pulses while keeping fiber length sufficiently large. Application of initial unchirped Gaussian pulses is preferable.

In the steady-state regime, Approach **B**, we obtain parabolic pulses with longer pulse duration (broadening factor ~5-6); however advantages here are the asymptotic properties of these pulses which are very similar to the similaritons in the fiber amplifier (excepting pulse amplification and spectral broadening). Application of initial chirped pulses is required; fiber length for femtosecond pulse formation is usually >10 cm.

7. Impact of higher order dispersion and nonlinear terms

Results presented in the preceding sections have been obtained within the frame of generalized propagation equation Eq. (1) which includes higher order dispersion terms (3-rd and 4-rd order dispersion), self-steepening and the intrapulse Raman scattering as compared to the standard NLSE. In this section we are presenting detailed analysis of influence of these higher order effects on fs-parabolic pulse shaping in Thorlabs 780 HP fiber. Analysis is presented for both approaches **A** and **B** under incidence of the Gaussian pulse. Results are presented in the form of maps of the misfit parameter like in preceding sections.

Figures 7(g1), 7(g2) shows the same maps of the misfit parameter as they are shown in Fig. 2(g1) and Fig. 3(g1) which include all effects (HN + HD). Also three maps are shown, which include only higher order dispersion effects (HD), higher order nonlinear effects (HN), and do not include any higher order effects (standard NLSE). As compared to Fig. 2(g1) and Fig. 3(g1) only contours of the maps are shown without filling which allows displaying of all maps together. Also Fig. 7(g1) is presented with a vertical axis in the logarithmic scale in order to show properly the high energy tail of HD and NLSE maps.

From Fig. 7(g1) we can see that in the transient regime the main feature is the appearance of sharp high energy tail in the NLSE and HD map. A similar high energy tail was observed previously by Finot at al. during the simulations of parabolic pulse formation using a standard NLSE [14]. The shape of NLSE-map tell us that standard NLSE overestimates energy of the incident pulse at short distances and also underestimate fiber length under real values of the maximal allowable pulse energies. Also NLSE overestimates maximal allowable fiber length. However, we can see that taking higher order dispersions into consideration reduces this tail down to 30 nJ (the peak of HD map), and inclusion of higher order nonlinearities reduces this high energy tail much stronger up to the 1.6 nJ (the peak of HN map). The physical meaning of this effect is that the action of high order dispersions and especially high order nonlinearities distorts the parabolic pulses shape at the high pump pulse energies, thus reducing the maximal energy of parabolic pulse formation. One can see that the action of

#189766 - $15.00 USD Received 30 Apr 2013; revised 3 Jun 2013; accepted 3 Jun 2013; published 18 Jul 2013
(C) 2013 OSA

higher order effects in the transient regime reduces also the maximal fiber's length where parabolic pulse is formed from 9 cm down to 8 cm.

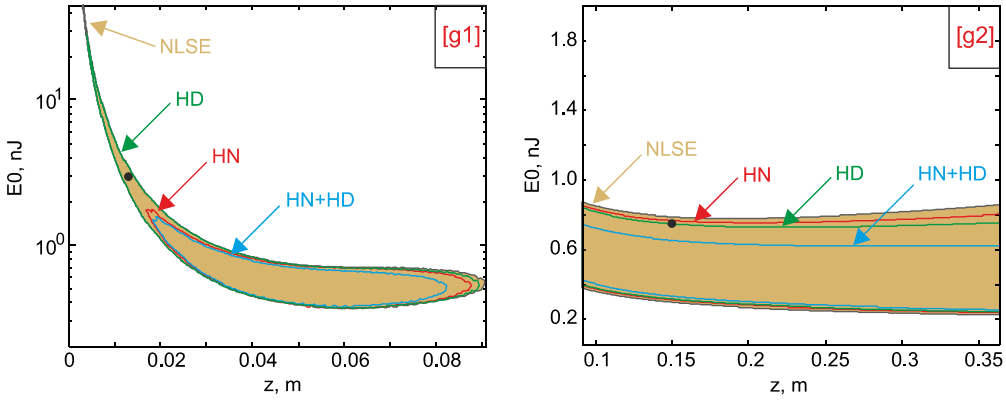

Fig. 7. Calculated contours of misfit parameter maps: (g1) - the transient regime (Approach (**A**) under incidence of unchirped 100 fs Gaussian pulse; (g2) - the steady-state regime (Approach (**B**) under incidence of chirped (C = 1.73) 100 fs Gaussian pulse. Contours of maps for the four cases are shown: NLSE – without any higher order effects, HD – only higher order dispersion effects are included, HN - only higher order nonlinear effects are included, HN + HD – all effects are included. Black dot denotes parameter set used in calculation of Fig. 8

In the steady-state regime shown in Fig. 7(g2) we can see that higher order effects also restrict maximal energy of the incident pulse form ~0.85 nJ down to ~0.65 nJ. The difference between full HN + HD map and HD or HN map shows that there is also a combined action of higher order nonlinear and dispersion effects leading to the stronger distortions of parabolic pulse shape as compared to separate action of higher order dispersion or nonlinearities. Such an action of nonlinearities at higher energies is naturally to expect because their impact directly depends on the peak power. The action of higher order dispersion we associate preliminary with a third order dispersion (TOD) which can introduce the steepening of the pulse shape in the steady-state regime [17]; the power of this distortion depends on the soliton order which is proportional to the pulse energy.

In order to better understand the deviation from parabolic shape introduced by higher order effects we have calculated pulse characteristics in the transient regime and in the steady-state one using set of parameters shown by black dots in Figs. 7(g1), 7(g2) respectively. The locations of these points were chosen outside of a full HN + HD map but inside of other maps, providing the better visibility of the distortions introduced by higher order nonlinear or dispersive effects which destroy parabolic pulse shape. Figure 8 shows wave forms and spectra of the pulses calculated at these points for all maps.

Pulse characteristics in the transient regime are shown in Figs. 8(g1), 8(g2). From these figures we can see that in the transient regime pulse characteristics HN and HN + HD are very close, the same one can see for NLSE and HD pulses. Thus the impact of higher order dispersion is very small here. Comparison of pulse shapes shown in Fig. 8(g1) shows us that the main distortions introduced by higher order nonlinear effects is a slight shifting of the pulse top toward the trailing edge and stronger steepening of pulse trailing edges of HN and HN + HD pulses as compared to the HD and NLSE pulses. Owing to that calculated misfit parameter of HD and NLSE pulses is parabolic ($M_{(\mathrm{HD})} = 0.036$, $M_{(\mathrm{NLSE})} = 0.036$), whereas inclusion of higher order effects leads to increasing of misfit parameter ($M_{(\mathrm{HN+HD})} = 0.046$, $M_{(\mathrm{HN})} = 0.045$). From the Fig. 8(g2) we can see that the main difference in the spectrum is asymmetry of HN and HN + HD pulses as compared to the HD and NLSE, the red-shifted peak is more intense than blue-shifted peak. These distortions of the pulse shapes and spectra are similar to that one produced by self-steepening effect [11]; therefore,

#189766 - $15.00 USD Received 30 Apr 2013; revised 3 Jun 2013; accepted 3 Jun 2013; published 18 Jul 2013
(C) 2013 OSA

we suppose that this high order nonlinear effect is a key reason of the visible pulse distortions.

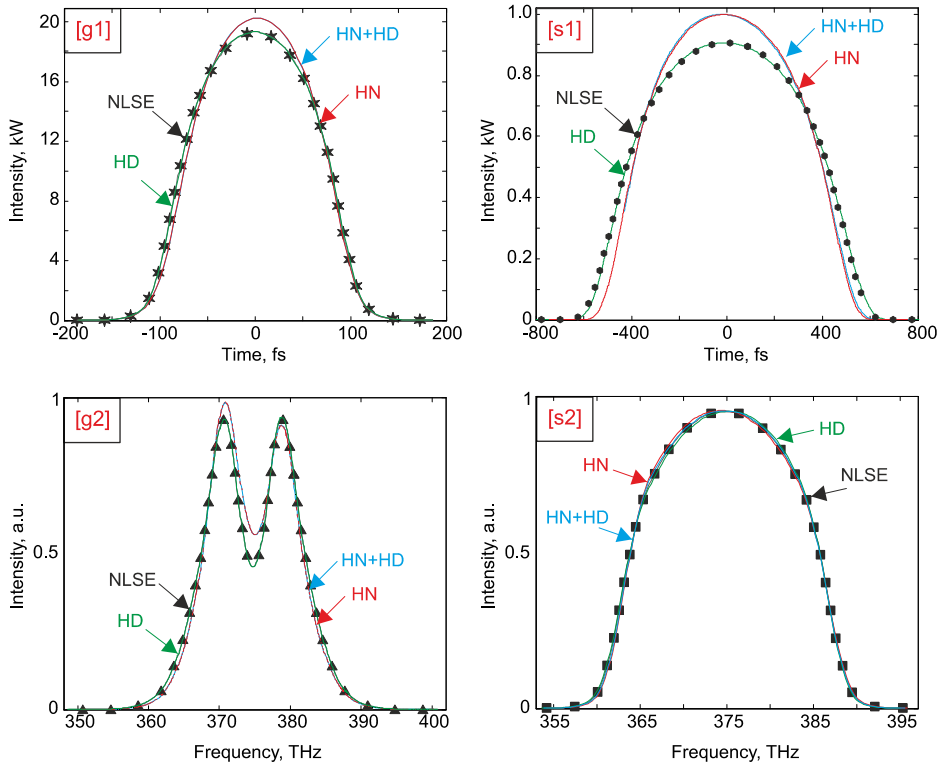

Fig. 8. Parabolic pulse shapes and spectra formed in the Thorlabs 780 HP at particular points of misfit parameter maps shown in Fig. 7 (g1), 7(s1). The left column shows results for parabolic pulse generated from initial unchirped Gaussian pulse ($\tau_0 = 100\,\text{fs}$, $E_0 = 3\,\text{nJ}$, $z = 1.3\,\text{cm}$). Right column shows parabolic pulse generated in the steady-state regime from initial chirped Gaussian pulse ($\tau_0 = 100\,\text{fs}$, $C = 1.73$, $E_0 = 0.75\,\text{nJ}$, $z = 15\,\text{cm}$). In both cases pulse characteristics are shown for all maps: NLSE, HD, HN and HN + HD.

In the steady-state regime the impact of higher order nonlinearities is reduced and becomes comparable with that one produced by higher order dispersions. Pulse shapes for all curves in the Fig. 8(s1) are nearly symmetrical without visible distortions. However, the shapes of spectra in the Fig. 8(s2) show better that slight asymmetry still exists. In spite of that both HD and HN pulses are parabolic ($M_{(\text{HD})} = 0.040$, $M_{(\text{HN})} = 0.038$) as well as the NLSE pulse ($M_{(\text{NLSE})} = 0.037$), whereas HD + HN pulse differs from a parabolic pulse shape ($M_{(\text{HN+HD})} = 0.044$). It means that separate action of higher order nonlinear and dispersive effects cannot distort sufficiently pulse shape from parabolic one, but their combined action can do.

Another important feature is that inclusion of higher order nonlinear effects into consideration results in decreased duration of the pulses regardless of its final shape. From Fig. 8(g1) one can see that HD and NLSE pulses is broadened stronger ($\tau_{(\text{HD})} = 161\,\text{fs}$, $\tau_{(\text{NLSE})} = 161\,\text{fs}$) as compared to the HN and HN + HD pulses ($\tau_{(\text{HN})} = 152\,\text{fs}$, $\tau_{(\text{HN+HD})} = 152\,\text{fs}$). The difference of pulse durations is 9 fs in this case. Figure 8 (s1) shows that in steady-state regime the compression effect is stronger. Pulse durations here are

#189766 - $15.00 USD Received 30 Apr 2013; revised 3 Jun 2013; accepted 3 Jun 2013; published 18 Jul 2013
(C) 2013 OSA

$\tau_{(HN+HD)} = 793$ fs, $\tau_{(HD)} = 876$ fs, $\tau_{(HN)} = 793$ fs, $\tau_{(NLSE)} = 876$ fs. The difference of pulse durations here is 83 fs. We suppose that this compression effect is related to the intrapulse Raman scattering. Previously it was shown that action of Raman scattering allows obtaining shorter pulses in the context of soliton pulse compression in fibers with anomalous dispersion [33], and particularly in the presence of negative TOD [34]. In the case of chirped pulse amplification it was shown that nonlinear phase shift induced by SPM in the normal dispersive case can be compensated by TOD of both signs producing shorter pulses [35]. In our case we have a normal dispersive fiber, but from Fig. 8 (g1) and 8(s1) we can see that similar compression appears both for HN and HN + HD pulses, i.e. it is actually independent on the presence of higher order dispersions. Therefore, we suppose that in our case the compression effect appears due to nonlinear phase shift induced by SPM is partly compensated by Raman scattering similarly to the action of 3-rd order dispersion in [35].

8. Conclusion

We have investigated numerically formation of femtosecond parabolic pulses by means of passive nonlinear reshaping in normal dispersive optical fibers. Parabolic pulse formation in different commercially available and theoretically designed fibers was analyzed applying initial pulses typical for modern femtosecond lasers. The ranges of pulse energy and fiber length providing parabolic pulse formation in the femtosecond time scale were found depending on the initial pulse duration, chirp and energy at 800 nm wavelength. Application of different fibers allows operating in the broad range of pulse energies. Particularly large mode area fibers can be used for producing nJ femtosecond parabolic pulses, whereas highly nonlinear fiber is better suited in the pJ range.

Two approaches were examined: parabolic waveform formation in transient and in the steady-state regimes. It has been shown that both approaches could provide parabolic pulse formation in the femtosecond time scale. Application of shorter initial pulses allows obtaining shorter parabolic pulses in the frame of both approaches. The advantage of the first approach is very short parabolic pulse formation with broadening factor approximately equal to ~2. Actually, the minimal width of parabolic pulses is limited only by the width of initial pulses and suitable short pieces (a few cm) of fiber. Application of initial unchirped pulses is preferable to obtain shortest pulses. In the steady-state regime we obtain parabolic pulses with longer pulse duration (broadening factor ~5-6); however advantages here are the asymptotic properties of these pulses, such as linear chirp, similar parabolic spectrum and stability of the pulse shape during further pulse propagation in the fiber. In this case application of initial chirped pulses is required; fiber length for femtosecond pulse formation has to be more than 10 cm.

The action of higher order nonlinear and dispersive effects on the femtosecond parabolic pulse formation is examined. It was shown that these effects restrict the maximal pulse energy of parabolic pulses due to the inducing of asymmetrical distortions of pulse shape. Another feature is found that inclusion of higher order nonlinearities results in shorter parabolic pulses with higher peak powers.

Acknowledgment

This work was supported by University of Guanajuato in the frame of DAIP grant 59/13 and by CONACyT within the sabbatical grant 175573/12. Financial support from the Ministerio de Economía y Competitividad and the Generalitat Valenciana of Spain (projects TEC2008-05490 and PROMETEO/2009/077, respectively).

#189766 - $15.00 USD Received 30 Apr 2013; revised 3 Jun 2013; accepted 3 Jun 2013; published 18 Jul 2013
(C) 2013 OSA